Spin Splitting of the Polaron Effective Mass in Triangular Quantum Well at Finite Temperature

X.-H. Wang[a] and Y.-J. Dai[b,*]

[a] *College of Sciences, Liaoning Petrochemical University, Fushun, Liaoning 113001, China*
[b] *College of Petroleum Engineering, Liaoning Petrochemical University, Fushun, Liaoning 113001, China*

Received: 11.06.2025 & Accepted: 23.07.2025

Doi: 10.12693/APhysPolA.148.68 *e-mail: keyanpaper2025@163.com

Based on the effective mass approximation theory and combining the linear combination operator with the unitary transformation method, the spin splitting characteristics of the polaron effective mass at finite temperatures were investigated. By introducing quantum statistical theory to describe the influence of thermally excited phonons, the functional relationships of the polaron effective mass with parameters such as temperature, electron–phonon coupling strength, and electron areal density were derived. Numerical calculations showed that the spin–orbit interaction leads to significant splitting of the polaron effective mass. The splitting distance increases with the increase in electron areal density, electron–phonon coupling strength, and vibration frequency, and decreases with the increase in velocity. An increase in temperature enhances electron–phonon interaction, leading to an increase in the polaron effective mass.

topics: temperature, spin splitting, effective mass, triangular quantum well

1. Introduction

Since the discovery of the tunnel magnetoresistance effect, spintronics has become one of the most popular fields of condensed matter physics. Spintronics differs from traditional electronics in that the spin of electrons is utilized as an additional degree of freedom, alongside their charge states [1–3]. The study of spintronics enables the fabrication of microelectronic components with epoch-making performance. By leveraging both the charge and spin of electrons for information transmission and storage, it can transform existing electronic devices from traditional electron injection to more efficient spin emission, doubling their operational efficiency [4, 5]. Therefore, we believe that microelectronic components based on spintronics will bring about tremendous changes in our lives. The foundation of spintronics lies in utilizing the fact that electrons with different spin states exhibit varying concentrations in different materials, giving rise to the phenomenon of spin-induced energy splitting [6]. It is obvious that an applied magnetic field can cause Zeeman energy splitting. When the inversion symmetry of the crystal structure is broken, even if the external magnetic field is shielded, the energy of electrons will still split. This splitting is different from the Zeeman splitting caused by an applied external magnetic field, and we call this splitting the Rashba spin–orbit splitting.

Datta et al. [7] first proposed the principle of a transistor based on controlling electron spin. This theory utilizes the Rashba effect in the semiconductor channel region to modulate the spin orientation of injected electrons [1]. Since Datta's article was published, numerous scholars internationally have conducted experimental [8, 9] and theoretical [10, 11] studies on the Rashba effect in low-dimensional quantum systems, particularly quantum well systems. For example, Qiu et al. [12] experimentally studied the beat frequency phenomenon in Shubnikov–de Haas oscillations of HgTe/HgCdTe quantum wells with inverted band structures. It has been demonstrated that the beat frequency phenomenon in HgTe quantum wells is caused by spin splitting generated by the Rashba effect. Xu et al. [13] theoretically calculated the spin–orbit splitting energy of electrons induced by the Rashba effect in asymmetric PbTe quantum wells using the four-band envelope wavefunction theory. They systematically discussed the dependence of

the spin splitting energy on critical structural parameters, including the quantum well growth orientation, degree of asymmetry, and well width. Due to the structural inversion asymmetry in semiconductor heterojunctions, electron spin degeneracy is lifted, leading to Rashba spin–orbit splitting of electrons at the Fermi surface. In narrow-bandgap semiconductors, electron spin splitting is predominantly induced by structural inversion asymmetry. Due to the asymmetric lattice structure of triangular quantum wells, phenomena such as spin–orbit coupling effects and rotational symmetry breaking of the spin Hamiltonian occur. In recent years, scholars have also conducted research on the Rashba spin–orbit splitting in triangular quantum wells. For instance, Li et al. [14] systematically investigated the Rashba effect on polarons in RbCl triangular quantum wells under magnetic fields via the Pekar variational method. Due to the Rashba effect, the ground-state energy of the polarons splits. It is indicated that the interaction of orbits and spins in different directions influences the energy of the polaron, which cannot be ignored. Using the improved linear combination operator method, Zhang et al. [15] investigated the Rashba spin–orbit splitting of the effective mass for a strongly coupled polaron in RbCl semiconductor triangular quantum wells. Under the Rashba spin–orbit interaction, the effective mass of the polaron also exhibits splitting. Although the spin splitting of the effective mass of the polarons in triangular quantum wells has been studied, the effect of temperature on the Rashba spin–orbit splitting of the polaron in triangular quantum wells remains uninvestigated to date.

2. Theoretical models and theoretical derivations

In the effective mass approximation, when an electron interacts with bulk longitudinal optical phonons in a triangular quantum well composed of two polar media, the Hamiltonian of the system can be expressed as

$$H = H_e + H_{\mathrm{LO}} + H_{\mathrm{LO-e}} + H_{\mathrm{SO}}, \tag{1}$$

where

$$H_e = \frac{p_{\parallel}^2}{2m} + \frac{p_z^2}{2m} + V(z), \tag{2}$$

$$H_{\mathrm{LO}} = \sum_k \hbar\omega_{\mathrm{LO}}\, a_k^{\dagger} a_k, \tag{3}$$

$$H_{\mathrm{LO-e}} = \sum_k \left(V_k\, a_k\, \mathrm{e}^{\mathrm{i}\boldsymbol{k}_{\parallel}\cdot\boldsymbol{\rho}+\mathrm{i}k_z z} + \mathrm{h.c.}\right), \tag{4}$$

$$H_{\mathrm{SO}} = \frac{a_{\mathrm{R}}}{\hbar}\left(\hat{\sigma}\times\hat{p}\right)_z. \tag{5}$$

The Hamiltonian H_e describes the energy of the electron. In (2), m is the band mass of the electron, and $V(z)$ is the bending potential of the electron conduction band. Under a large negative bias voltage, this potential energy is approximately triangular, and it is also known as the triangle potential

$$V(z) = \begin{cases} eF_s\, z, & z > 0, \\ \infty, & z \le 0, \end{cases} \tag{6}$$

and

$$F_s = \frac{4\pi e\, n_s}{\varepsilon_{01}}. \tag{7}$$

Here, F_s represents the built-in electric field, n_s represents the electron surface density, and ε_{01} is the static dielectric constant.

The Hamiltonian H_{LO} describes the energy of the bulk longitudinal optical phonon field, ω_{LO} is the frequency of the longitudinal optical (LO) phonon, and $a_k^{\dagger}$ (a_k) is the creation (annihilation) operator of the bulk longitudinal optical phonon with wave vector $\boldsymbol{k}$.

The Hamiltonian $H_{\mathrm{LO-e}}$ describes the interaction energy between the electron and the bulk longitudinal optical phonon, and $\boldsymbol{r} = (\boldsymbol{\rho}, z)$ is the electron's coordinate vector. The interaction Fourier coefficient is

$$V_k = \mathrm{i}\left(\frac{\hbar\omega_{\mathrm{LO}}}{k}\right)\left(\frac{\hbar}{2m\,\omega_{\mathrm{LO}}}\right)^{1/4}\left(\frac{4\pi\alpha}{V}\right)^{1/2}. \tag{8}$$

Here, V is the volume of the crystal, and the electron-LO phonon coupling constant is represented by α, which depends on the material of the quantum well.

The Hamiltonian H_{SO} describes the spin–orbit interaction energy, where α_{R} is the spin–orbit coupling constant, which is proportional to $\frac{\partial V(z)}{\partial z}$. Here, $V(z)$ includes both the electron confinement potential and the external electric field potential. A linear combination operator is introduced for the momentum and coordinates of the transverse motion of the electron, respectively,

$$p_j = \sqrt{\frac{m\hbar\,\lambda}{2}}\left(b_j + b_j^{\dagger} + p_{0j}\right), \tag{9}$$

and

$$\rho_j = \mathrm{i}\sqrt{\frac{\hbar}{2m\,\lambda}}\left(b_j - b_j^{\dagger}\right), \tag{10}$$

($j = x, y$), where λ is a variational parameter and represents the polaron vibration frequency.

Under the adiabatic approximation, a unitary transformation is performed on the Hamiltonian H. The unitary transformation operator is chosen as

$$U = \exp\left[\sum\nolimits_k \left(a_k^{\dagger} f_k - a_k f_k^{*}\right)\right]. \tag{11}$$

In the above equation, f_k and f_k^{*} are variational parameter functions. By taking the variation of energy with respect to f_k and f_k^{*} and then taking the limit, the expressions of f_k^{*} and f_k can be obtained.

Let us select the trial wave function for the ground state of the system as

$$|\psi\rangle = |\phi(z)\rangle\left(a\,\chi_{1/2} + b\,\chi_{-1/2}\right)|0\rangle_a|0\rangle_b. \tag{12}$$

Here, $|0\rangle_b$ is the vacuum state of the operator b, and $|0\rangle_a$ is the zero-phonon state, which satisfies the conditions $b_j\,|\rangle_b = 0, a_k\,|\rangle_a = 0$. The spin-down state is represented by $\chi_{-1/2} = [0,\ 1]^{\mathrm{T}}$, and the spin-up state is represented by $\chi_{1/2} = [1,\ 0]^{\mathrm{T}}$. Both a and b are coefficients. In turn, $|\phi(z)\rangle$ is the wave function of the triangular quantum well moving in the z-direction. We choose the Fang–Howard variational wave function as follows

$$\phi\,(z) = \begin{cases} \sqrt{\dfrac{d^3}{2}}\, z \exp\left(-\dfrac{d}{2}\right), & z > 0, \\ 0, & z \le 0, \end{cases} \tag{13}$$

where d is a variational parameter. It is varied by the total energy of the system and obtained by taking the minimum value.

The total momentum of the system is

$$\boldsymbol{P}_{\parallel,\mathrm{tot}} = \boldsymbol{p}_{\parallel} + \sum_k \hbar k\, a_k^{\dagger} a_k. \tag{14}$$

In order to determine the effective mass of the polaron, we need to find the expectation value of $|\phi\rangle$ with respect to $U^{-1}(H - \boldsymbol{u}\cdot\boldsymbol{P}_{\parallel,\mathrm{tot}})\ U$. Here, $\boldsymbol{u}$ is the Lagrangian multiplier, which is used to represent the velocity of the polaron. Then we obtain

$$F(u, p_0, \lambda, d, f_k) = \langle\psi|\, U^{-1}\Big(H - \boldsymbol{u}\cdot\boldsymbol{P}_{\parallel,\mathrm{tot}}\Big) U\,|\psi\rangle\,. \tag{15}$$

Then, by taking the variations of the parameters f_k, p_0, λ, and d in (15) and finding the extreme values, we can obtain the effective mass of the polaron in the triangular quantum well. The expected value of the momentum of the polaron is obtained as

$$p_{\parallel} = m\left[1 + \frac{\sqrt{\pi}\alpha}{2}\left(\frac{\lambda}{\omega_{\mathrm{LO}}}\right)^{3/2} \pm \frac{2a_{\mathrm{R}}}{\hbar u}\right] u. \tag{16}$$

It can be seen from (16) that the effective mass of the polaron is

$$m^* = m\left[1 + \frac{\sqrt{\pi}\alpha}{2}\left(\frac{\lambda}{\omega_{\mathrm{LO}}}\right)^{3/2} \pm \frac{2a_{\mathrm{R}}}{\hbar u}\right]. \tag{17}$$

Then we calculate the mean number of phonons, i.e.,

$$N = \langle\psi|U^{-}\sum_k a_k^{\dagger} a_k\, U|\psi\rangle = \frac{1}{2}\,\alpha\hbar\sqrt{\pi\,\lambda\,\omega_{\mathrm{LO}}}. \tag{18}$$

At finite temperatures, the electron–phonon system will no longer be completely in the ground state. Lattice vibration not only excites real phonons but also causes the electrons to be excited. The properties of the polaron are determined by the statistical average values of the electron–phonon system for various states. According to quantum statistics, the mean number of phonons can also be expressed as

$$\bar{N} = \left[\exp\left(\frac{\hbar\omega_{\mathrm{LO}}}{K_{\mathrm{B}}T}\right) - 1\right]^{-1}. \tag{19}$$

In (19), K_{b} is the Boltzmann constant with value 1.38×10^{-23} J/K. The value of λ in (18) is related not only to N but also to $\bar{N}$.

3. Numerical calculation and discussion

We theoretically derived expressions for the effective mass of the polaron and the mean number of phonons in a triangular quantum well using a combination of an improved linear combination operator method and unitary transformation. By incorporating the expression for the mean number of phonons from quantum statistical mechanics, the functional relationship between the polaron effective mass and temperature was derived. To clearly illustrate the effects of temperature and spin–orbit interaction on the effective mass of the polaron, numerical calculations were performed using polaron units. The results are presented in the following five figures.

Figure 1 depicts the curves showing the relationship between the polaron effective mass m^* and the electron–phonon coupling strength α, with the electron surface density n_s set to 2 and 3. As can be seen in the figure, the effective masses of the polaron in different spin states are clearly separated. It indicates that the spin–orbit interaction causes the splitting of the effective mass of the polaron. In Fig. 1, the solid line represents the zero-spin effective mass m_0^*, the dashed line represents the spin-up split effective mass m_+^*, and the dotted line represents the spin-down split effective mass m_-^*. As can be seen, for both $n_s = 2$ and $n_s = 3$, the effective mass corresponding to each curve increases with the increase in α. This is because the stronger the electron–phonon coupling, the greater the influence of phonon dragging on the electron moving in the lattice. For this reason, the effective mass of the polaron increases with the increase in the strength of electron–phonon coupling. At the same electron–phonon coupling strength, the larger the electron areal density, the greater the splitting distance of the effective mass of the polaron.

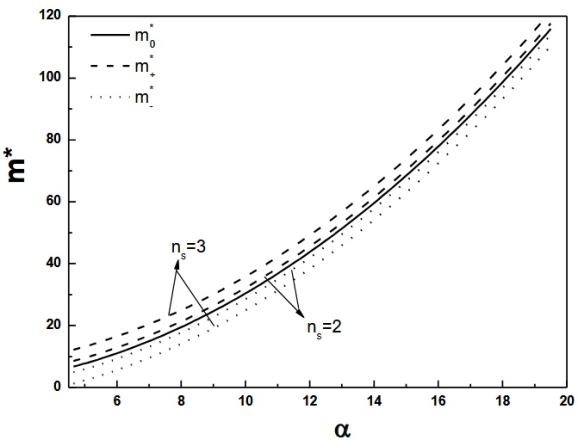

Fig. 1. The effective mass m^* versus the electron–phonon coupling strength α with different electron surface densities n_s.

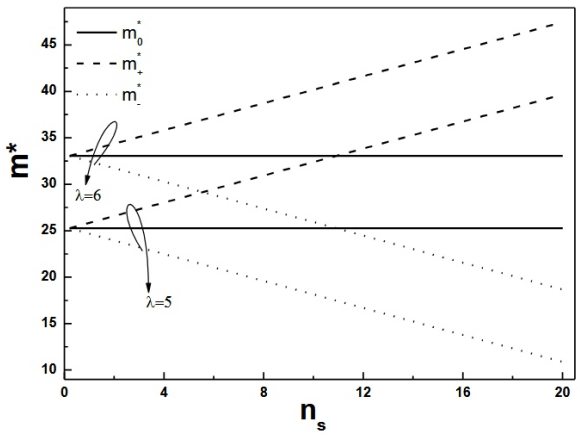

Fig. 2. The effective mass m^* versus the electron surface density n_s with different vibration frequencies λ.

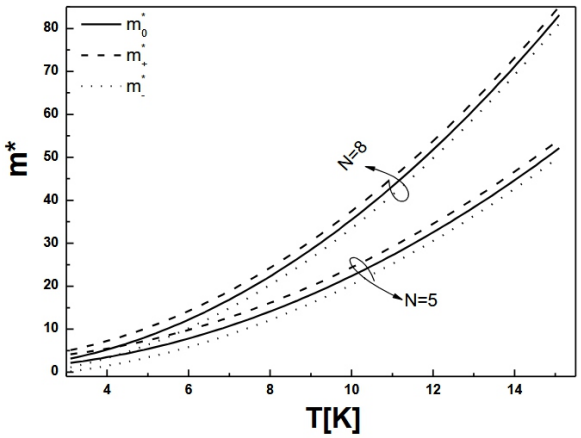

Fig. 3. The effective mass m^* versus the temperature T with different mean number of phonons N.

Figure 2 illustrates the variation of the polaron effective mass m^* with the electron areal density n_s when the spin–orbit interaction is considered and the polaron vibration frequency λ takes different values. As can be seen in the figure, due to the spin–orbit interaction, the effective mass of the polaron splits based on the zero-spin state. In Fig. 2, the solid line represents the zero-spin effective mass m_0^*, the dashed line represents the spin-up split effective mass m_+^*, and the dotted line represents the spin-down split effective mass m_-^*. When the electron areal density is fixed, the higher the vibration frequency, the larger the effective mass of the polaron. This is because the more intense the phonon vibration, the more frequent the interaction between the electron and phonon. In other words, the electron–phonon coupling strength is related to the vibration frequency, and a higher vibration frequency corresponds to a stronger electron–phonon coupling. Therefore, as the vibration frequency increases, the effective mass of the polaron increases. When the electron areal density $n_s = 0$, the effective mass does not exhibit splitting. As the electron areal density increases, the splitting of the effective mass becomes increasingly obvious. This is because the spin–orbit coupling constant α_{R} is proportional to $\frac{\partial V(z)}{\partial z}$. It follows from (6), (7), and (17) that the effective mass is proportional to the electron surface density. Therefore, in Fig. 2, both the spin-up and spin-down split effective masses exhibit a linear change with the electron areal density, and the splitting distance increases as the electron areal density rises.

Figure 3 depicts the variation of the polaron effective mass m^* with temperature T under different mean number of phonons N when the spin–orbit interaction is considered. As can be seen from the figure, the effective mass curves of the polaron in different spin states are clearly separated, indicating that the spin–orbit interaction causes the effective mass of the polaron to split. In Fig. 3, the solid line represents the zero-spin effective mass m_0^*, the dashed line represents the spin-up split effective mass m_+^*, and the dotted line represents the spin-down split effective mass m_-^*. Under different spin states, the interactions between the electron and phonons, as well as their motion within the lattice, exhibit distinct characteristics, thereby giving rise to different effective masses of the polaron. And during the changes in temperature and mean number of phonons, the difference in effective mass caused by spin–orbit interaction always exists. For a given mean number of phonons N and spin state, the effective mass of the polaron m^* increases with the rise in temperature T. As the temperature rises, the thermal excitation of phonons intensifies, leading to more frequent and stronger interactions between electron and phonons. This increased interaction enhances the obstruction to electron movement within the lattice, thereby causing the effective mass of the polaron to increase. As can be seen in Fig. 3, for any spin state, the effective mass corresponding to each curve increases with rising temperature. At the same temperature T and spin state, the larger the mean number of phonons N, the greater the effective mass of polaron m^+. This is because a larger mean number of phonons implies a stronger interaction between phonons and electron, which imposes greater hindrance on electron movement, thereby leading to an increase in the effective mass of the polaron.

Figure 4 illustrates the variation of the polaron effective mass m^* with temperature T under different electron areal densities when spin–orbit interaction is considered. The effective mass curves of the polaron in different spin states are clearly separated, indicating that the spin–orbit interaction causes the splitting of the polaron effective mass. In Fig. 4, the solid line represents the zero-spin effective mass m_0^*, the dashed line represents the spin-up

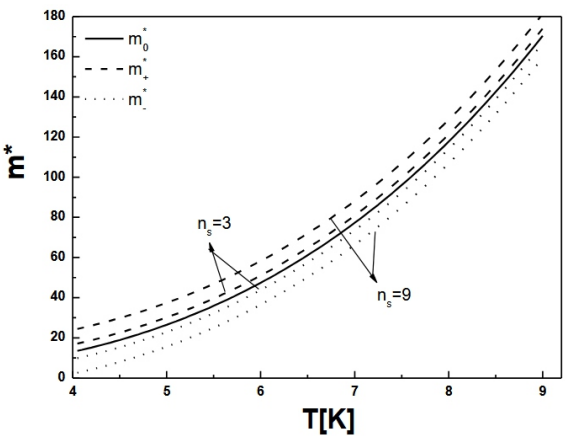

Fig. 4. The effective mass m^* versus the temperature T with different electron surface densities n_s.

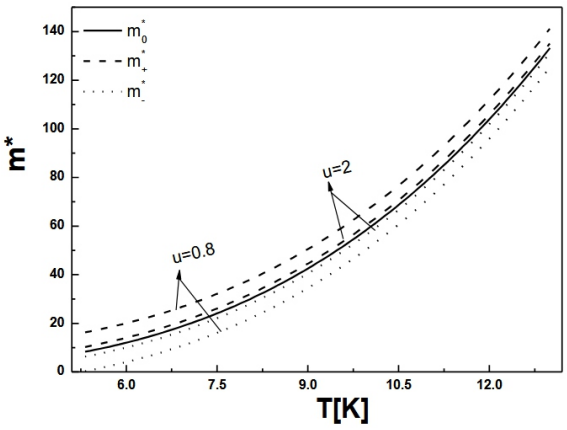

Fig. 5. The effective mass m^* versus the temperature T with different velocities u.

split effective mass m_+^*, and the dotted line represents the spin-down split effective mass m_-^*. For a given electron areal density n_s and spin states (corresponding to different curves m_0^*, m_+^*, m_-^*), the effective mass of the polarons m^* increases with the rise in temperature T. As the temperature increases, the thermal vibration of phonons intensifies, enhancing the interaction between the electron and phonons. This leads to an increase in scattering effects on electron movement within the lattice, thereby causing the effective mass of the polaron to rise. At the same temperature T and spin state, the larger the electron areal density n_s, the greater the effective mass of the polaron m^*. This is because as the electron areal density increases, the interaction between the electron and phonons becomes more complex, imposing more constraints on electron movement within the lattice. Consequently, the effective mass of the polaron increases due to these enhanced interactive constraints.

Figure 5 depicts the variation of the polaron effective mass m^* with temperature T under different polaron velocities u when the spin–orbit interaction is considered. As can be seen in the figure, for any spin state, the effective mass corresponding to each curve increases with the rise in temperature. When the temperature is fixed, the smaller the polaron velocity, the larger the splitting distance of the effective mass. As the polaron velocity increases, the electron–phonon interaction weakens. Since the electron–phonon interaction has a positive contribution to spin splitting, an increase in velocity diminishes the splitting of the effective mass. In (17), the velocity is inversely proportional to the spin-split effective mass, leading to the conclusion that an increase in velocity results in smaller spin splitting of the effective mass.

4. Conclusions

Based on the effective mass approximation theory and combining the linear combination operator with the unitary transformation method, the spin splitting characteristics of the polaron effective mass at finite temperatures were investigated. The effective mass curves of the polarons in different spin states are clearly separated, indicating that the spin–orbit interaction causes the splitting of the effective mass of the polaron in a triangular quantum well. In different spin states, the electron–phonon interaction and the lattice motion of the electron exhibit distinct characteristics, thereby giving rise to variations in effective mass. The increase in electron surface density further widens the spin-splitting distance by enhancing the built-in electric field, indicating that structural parameters can effectively regulate spin-related effects. An increase in temperature enhances the thermal excitation of phonons, intensifying electron–phonon interaction and increasing the resistance to electron motion in the lattice, thereby causing the polaron effective mass to rise monotonically with temperature.

Acknowledgments

This work was supported by the Key Scientific and Technological Research Project of Liaoning Provincial Department of Education (Grant No. LJKZZ202200547).

References

[1] E.I. Rashba, A.L. Efros, *Phys. Rev. Lett.* **91**, 126405 (2003).

[2] S.A. Wolf, D.D. Awschalom, R.A. Buhrman, J.M. Daughton, S. von Molnár, M.L. Roukes, A.Y. Chtchelkanova, D.M. Treger, *Science* **294**, 1488 (2001).

[3] D. Culcer, J. Sinova, N.A. Sinova, T. Jungwirth, A.H. MacDonald, Q. Niu, *Phys. Rev. Lett.* **93**, 046602 (2004).

[4] S.-P. Shan, S.-H. Chen, *J. Low Temp. Phys.* **197**, 379 (2019).

[5] S.-P. Shan, S.-H. Chen, J.-L. Xiao, *J. Low Temp. Phys.* **175**, 523 (2014).

[6] W. Xuan, N. Yang, J. Luo, R. Wang, H. Yang, G. Jin, *Appl. Phys. A* **129**, 88 (2023).

[7] S. Datta, B. Das, *Appl. Phys. Lett.* **56**, 665 (1990).

[8] C.X. Zhang, A. Pfeuffer-Jeschke, K. Ortner, C.R. Becker, G. Landwehr, *Phys. Rev. B* **65**, 5324 (2002).

[9] F. Meng, J. Zhao, J. Cheng, W. Liu, *Phys. B* **649**, 414468 (2023).

[10] S.-P. Shan, S.-H. Chen, *Pramana J. Phys.* **94**, 15 (2020).

[11] J.P. Stanley, N. Pattinson, C.J. Lambert, J.H. Jefferson, *Physica E* **20**, 433 (2004).

[12] Z.-J. Qiu, Y.-S. Gui, X.-Z. Shu, N. Dai, S.-L. Guo, J.-H. Chu, *Acta Phys. Sin.* **53**, 1186 (2004).

[13] T.-N. Xu, H.-Z. Wu, C.-H. Sui, *Acta Phys. Sin.* **57**, 7665 (2008).

[14] Y.-L. Li, S.-P. Shan, *Acta Phys. Pol. A* **146**, 129 (2024).

[15] Z. Hai-Rui, X. Jing-Lin, *Commun. Theor. Phys.* **50**, 995 (2008).